International Journal of Heat and Mass Transfer 127 (2018) 607–613

Contents lists available at ScienceDirect

International Journal of Heat and Mass Transfer

journal homepage: www.elsevier.com/locate/ijhmt

Thermal illusion with twinborn-like heat signatures

Shuling Zhou, Run Hu *, Xiaobing Luo

School of Energy and Power Engineering, Huazhong University of Science and Technology, Wuhan 430074, China

ARTICLE INFO

Article history:
Received 9 May 2018
Received in revised form 28 June 2018
Accepted 7 July 2018

ABSTRACT

Thermal illusion device, which can change an arbitrary object into another one when observed from an infrared vision, recently has attracted considerable attention amongst a series of innovative thermal phenomena by resorting to the unique thermal metamaterial. To enhance the illusion deceptiveness, current thermal illusion devices mostly change the location or shape of the target, but seldom deal with the number of heat signatures. In this paper, we develop a general formula to enhance the illusion deceptiveness by splitting the thermal target to appear like thermal bilocation with twinborn distinct heat signatures. The exhaustive design process based on transformation thermodynamics is rigorously introduced in order to realize thermal bilocation. Simulative and experimental results agree well with each other and validate the conception of thermal bilocation. Additionally, the influence of three structure parameters on the bilocation effects has been considered for further optimization. Our device can thermally camouflage the original target with twinborn signatures at different locations, improving the deceptiveness greatly compared with only moving or reshaping. The present thermal bilocation not only can fortify the performance of thermal camouflage, but also can stimulate the extension of illusion thermodynamics to further physical applications.

1. Introduction

When it comes to camouflage, people may think up with some animals in natural biology, like chameleon and octopus, which possess the amazing color-change ability by changing their skins to replicate the color of its surroundings adaptively. Analogous with color-change camouflage in visible spectrum, temperature change of the appearance of cold-blooded animals in infrared vision actually have enlightened researchers of the thermal camouflage. After a long term of research, the form invariance of governmental equation under coordinate transformation between different spaces has been confirmed to be feasible in the implementation of optical transformation [1,2] and thermal transformation [3–8], giving birth to two new disciplines named as transformation optics (TO) and transformation thermodynamics (TTD), respectively. Based on the rapid development of TTD, many new heat transfer phenomena with characteristic functions have been reported theoretically or experimentally, such as thermal cloaks [9–15], concentrators [16], rotators [17], reversers [18], diodes [19], refractors [20], lens [21,22], trapping [23], camouflage [24–28] and illusion [29–31], etc. At present, thermal illusion has become one of the most fabulous and appealing phenomena, which in broad sense includes thermal cloaking and thermal camouflage, seeming quite promising in the contemporary life and military applications. While existing thermal illusions just consider the changing of heat target's location [26] or shape [30], seldom could deal with the number of heat signatures. Our recent paper [31] sheds light on such challenge and provides a general strategy to deal with the number of heat signatures. The consequent function can be called as thermal bilocation [32] which means the target seems to be found in two distinct places at the same time in infrared vision. However, the strategy has not been intensively explored and the performance can be optimized further. In this paper, we strive to design a thermal meta-device with the function of thermal bilocation based on the transformation thermodynamics to relocate the separated heat sources, and experimentally demonstrate the interesting twinborn thermal performance.

2. Methodology

2.1. Transformation thermodynamics (TTD)

Guided by the theory of TTD, we first demonstrate a general linear coordinate transformation method to move a target inside a rectangular plane *OBCD* [26]. As shown in Fig. 1, the original rectangular target *PQMN* is moved to the new place as rectangular *P′Q′M′N′*, and the whole plane is divided into four trapezoidal sections (denoted as 1, 2, 3 and 4) respectively, instead of the triangular partition in Ref. [31]. The dimensions of the plane *OBCD*

* Corresponding author.
E-mail address: hurun@hust.edu.cn (R. Hu).

https://doi.org/10.1016/j.ijheatmasstransfer.2018.07.034
0017-9310/

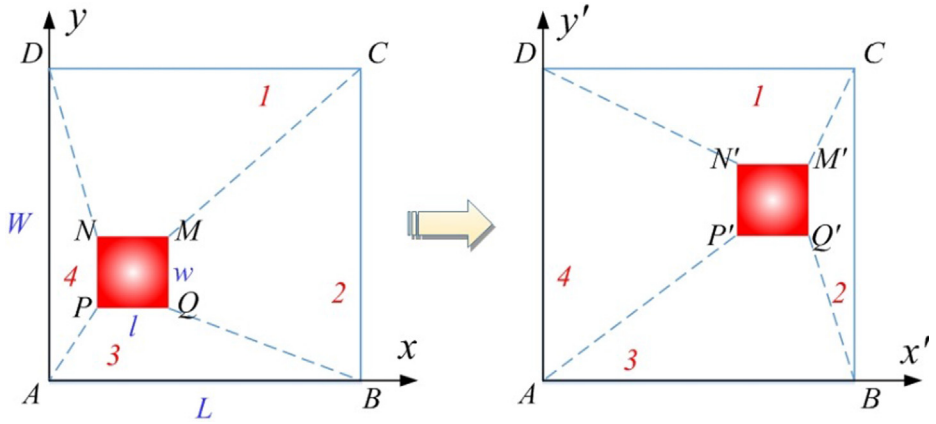

Fig. 1. Schematic of moving target based on linear transformation.

and the target are $L \times W$ and $l \times w$, respectively. Each point (x, y) in the trapezoidal section is then mapped to new one (x', y') in the corresponding trapezoidal section by following linear transformation, as

$$\begin{bmatrix} x'_n \\ y'_n \\ 1 \end{bmatrix} = \begin{bmatrix} \alpha_n & \beta_n & \gamma_n \\ \mu_n & \nu_n & \varepsilon_n \\ 0 & 0 & 1 \end{bmatrix} \begin{bmatrix} x_n \\ y_n \\ 1 \end{bmatrix} \tag{1}$$

where α_n, β_n, γ_n, μ_n, ν_n, and ε_n are the six undetermined coefficients, subscript index n denotes the nth trapezoidal section, and the superscript denotes the transformed space. Since we can design the coordinates of the original and the moved targets, the six coefficients of each trapezium section can be easily obtained as a result of substituting its own any three vertexes into Eq. (1), as indicated in Table 1. With this general method, we can move the target to almost anywhere desired.

According to the Fourier law of heat conduction, the heat flux in the ith direction (q_i) under a given temperature gradient in the jth direction (∇T_j) can be expressed as $q_i = -\kappa_{ij}\nabla T_j$, where κ_{ij} $\left(= \begin{bmatrix} \kappa_{xx} & \kappa_{xy} \\ \kappa_{yx} & \kappa_{yy} \end{bmatrix}\right)$ is the second-order thermal conductivity tensor of the materials. Based on the principle of the transformation thermodynamics, the Fourier equation maintains form invariant after coordinate transformation, however an adjustment arises on the thermal conductivity tensor from the virtual space (x, y) to the real space (x', y'), which can be expressed as

$$\kappa'_n = \kappa'_{nij} = \begin{bmatrix} \kappa'_{nxx} & \kappa'_{nxy} \\ \kappa'_{nyx} & \kappa'_{nyy} \end{bmatrix} = \frac{J_n \kappa_0 J_n^T}{\det(J_n)} \tag{2}$$

where κ_0 is the homogeneous thermal conductivity in the virtual space and J_n is the Jacobian matrix of the coordinate transformation in nth section, as

$$J_n = \frac{\partial(x'_n, y'_n)}{\partial(x_n, y_n)} = \begin{bmatrix} \frac{\partial x'_n}{\partial x_n} & \frac{\partial x'_n}{\partial y_n} \\ \frac{\partial y'_n}{\partial x_n} & \frac{\partial y'_n}{\partial y_n} \end{bmatrix} = \begin{bmatrix} \alpha_n & \beta_n \\ \mu_n & \nu_n \end{bmatrix}. \tag{3}$$

Based on the coefficients listed in Table 1, we can calculate the transformed thermal conductivity tensors of each section according to Eq. (2) [3–6], and the results are listed in Table 2. With such transformed thermal conductivity tensors, we can try to realize the function of thermal bilocation.

Now we establish the design of thermal bilocation device with twinborn heat signatures. As shown in Fig. 2(a), the Cartesian coordinate systems coincide with each other in both virtual space and real space at point O. The x-y (x'-y') axis divides the actual target (blue[1] rectangle) into four subsections. Taking the first quadrant as an example, its subsection of the virtual target is the rectangular $PQMN$ which we move to the rectangular $P'Q'M'N'$ in the way of above general thermal moving with corresponding six coefficients. Note that (1) the point P' coincides with point O and (2) the segment PQ overlaps with the x-axis. With such a transformation, the target in real space can represent two signatures (red rectangle) in the virtual space, on account of the two thermal moving which occur respectively and simultaneously in the two subsections of the real target. The thermal conductivity tensors in each section with distinct design parameters are obtained and listed in Table 2. Note that our design does not require the symmetry of structure, which means the original heat source (blue rectangle) can be located anywhere in the device. Fig. 2(b) shows the asymmetric design with four different size sections instead of the same size ones of the symmetric design. By far, it's ready for the simulative and experimental verifications of the thermal bilocation prototype.

3. Experiments and simulations

As for the prototypes, we fabricated symmetry samples for thermal-bilocation demonstrations and the #45 carbon steel (κ_m = 49.8 W/(m K)) is chosen as the substrate. The dimensions for the thermal-bilocation substrates are 160 mm × 120 mm × 2 mm. Our previous study suggests the thickness of the substrate [36]. The substrate possesses two feet at the two sides for water-bath experiments. Due to axial symmetry of the device, thermal conductivities in each quadrant are axially symmetric. Here we just design the part of the first quadrant where the dimensions for the thermal-bilocation region and the target heat source are L = 40 mm, W = 22.3 mm, l = 10 mm, w = 5 mm, respectively. The point P (c, d) of the heat signature is placed at (20, 0) mm. Since the point P' of the signatures are located at the original point O, only the subsection 1 and 2 exist and need designing. Moreover, according to simplification progress of anisotropic thermal conductivities, when the structure parameters in our cases meet the relationship as $(L-l)^2 - (W-w)^2 = c(L-l)$, thermal conductivity tensors at subsection 1 and 2 are the same as $\kappa_0 \begin{bmatrix} 3 & 0 \\ 0 & 1/3 \end{bmatrix}$ W/(m K) but with different rotation angles as 30° and 0° respectively. Similar to the experimental process in our recent paper

[1] For interpretation of color in Figs. 2, 3, 4 and 8, the reader is referred to the web version of this article.

Table 1
Six coefficients of the linear transformation in each section according to Eq. (1).[a]

Section n	α_n	β_n	γ_n	μ_n	ν_n	ε_n
1	1	$-\frac{c-a}{W-w-b}$	$\frac{W(c-a)}{W-w-b}$	0	$\frac{W-w-d}{W-w-b}$	$\frac{W(d-b)}{W-w-b}$
2	$\frac{L-l-c}{L-l-a}$	0	$\frac{L(c-a)}{L-l-a}$	$-\frac{d-b}{L-l-a}$	1	$\frac{L(d-b)}{L-l-a}$
3	1	$(c-a)/b$	0	0	d/b	0
4	c/a	0	0	$(d-b)/a$	1	0

[a] (a, b) and (c, d) are the coordinate of Points P and P' respectively.

Table 2
Transformed thermal conductivity tensors in each section.

Section n	κ'_n	Section n	κ'_n
1	$\kappa_0\begin{bmatrix}\frac{(c-a)^2+(b+w-W)^2}{(b+w-W)(d+w-W)} & \frac{c-a}{b+w-W}\\ \frac{c-a}{b+w-W} & \frac{d+w-W}{b+w-W}\end{bmatrix}$	3	$\kappa_0\begin{bmatrix}\frac{(c-a)^2+b^2}{bd} & (c-a)/b\\ (c-a)/b & d/b\end{bmatrix}$
2	$\kappa_0\begin{bmatrix}\frac{c+l-L}{a+l-L} & \frac{d-b}{a+l-L}\\ \frac{d-b}{a+l-L} & \frac{(d-b)^2+(a+l-L)^2}{(a+l-L)(c+l-L)}\end{bmatrix}$	4	$\kappa_0\begin{bmatrix}c/a & (d-b)/a\\ (d-b)/a & \frac{(d-b)^2+a^2}{ac}\end{bmatrix}$

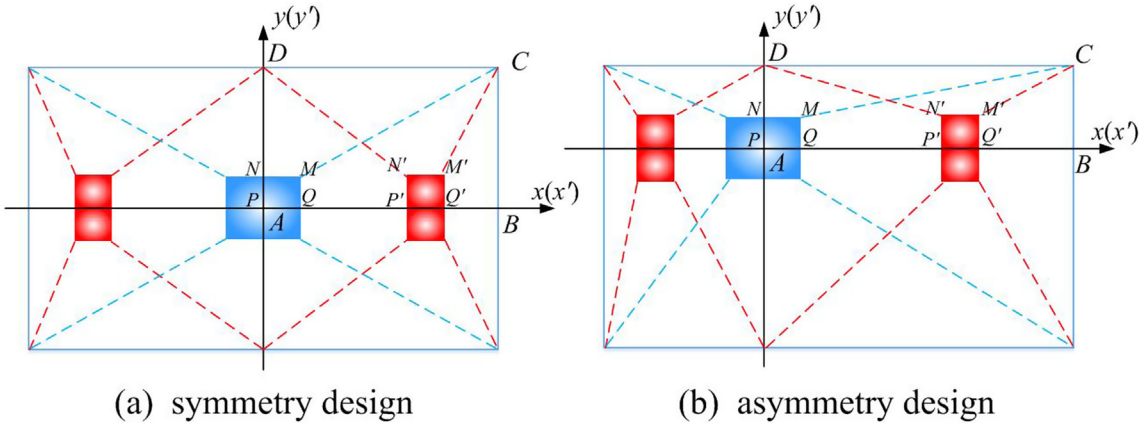

Fig. 2. Design schematics of thermal bilocation, (a) symmetric design (b) asymmetric design.

[31], we can use the effective medium theory (EMT) to realize the inhomogeneous thermal conductivity tensor. As illustrated in Fig. 3, the engineering composite consists of two kinds of materials just with consistent thermal conductivity and have easier process ability compared to the common-used layered composites [33,34] and the particle composites [35]. When the filling ratio of the filling material is f, and the thermal conductivity of the matrix material and filling materials are κ_m and κ_f respectively, the effective thermal conductivity along x'-axis is $\kappa_{x'} = f\kappa_f + (1-f)\kappa_m$, while the effective conductivity along y'-axis is $\kappa_{y'} = (f/\kappa_f + (1-f)/\kappa_m)^{-1}$. With $\begin{bmatrix}\kappa_{x'} & 0\\ 0 & \kappa_{y'}\end{bmatrix}$, we can realize the equivalent inhomogeneous thermal conductivity tensors in Table 2. By equaling the simplified thermal conductivity tensor to the

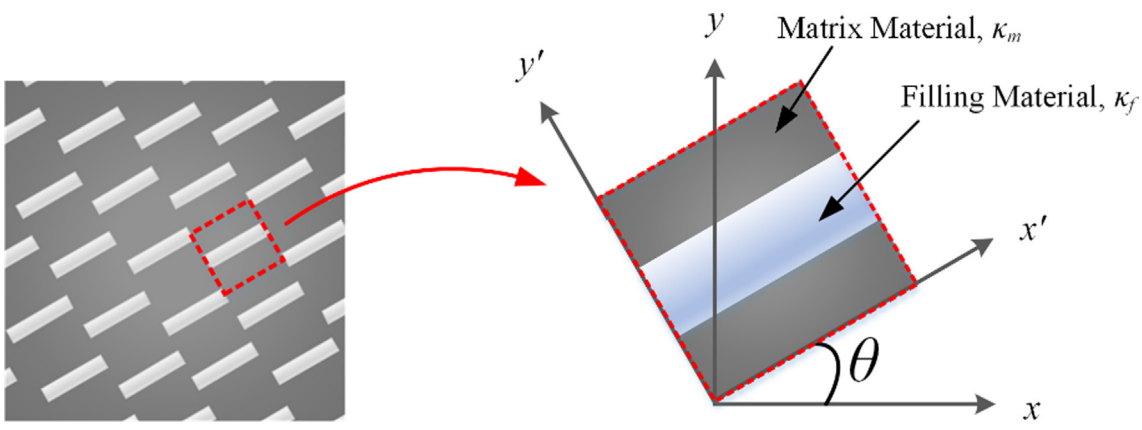

Fig. 3. Schematic of the engineering composite.

experimental filling one, we obtained that the thermal conductivity of the background κ_0 was 33.8 W/(m K) as well as the corresponding filling ratio f was 0.33 and thermal conductivity of the filling material κ_f was 1.3 W/(m K). The manufacturing method and progress were outlined in our reported study [31]. Uniform holes with a radius of 2.8 mm and the pitch of 10 mm are drilled in background, meanwhile rectangular holes, with the varied rotated angle, the same size of 10 mm × 3.3 mm and the same pitch of 10 mm, are drilled in each subsections of the thermal bilocation region. Required filling material is the composite of epoxy and hexagonal boron nitride (hBN) particles with 15% volume fraction [37], calibrated with Laser Flash Analyzer (LFA 467). In Fig. 3, the left (right) white rectangles (due to the color of the epoxy-based mixture) in the thermal bilocation region are the filled rectangular holes, whose orientation and filling materials are well consistent with the above design.

In the experiments, the samples were maintained horizontally and the left and right feet were immersed in the mixture of ice and water, i.e. at zero Celsius degree. Square ceramic heaters were used as heat sources with size of 10 mm × 10 mm, electric resistance of 5 Ω, nominal voltage of 4.2 V. All the heaters worked at constant voltage of 4.2 V from a constant voltage DC source. To maintain the constant thermal emissivity, all the samples were wrapped with the same kind of transparent adhesive tape. An IR camera (FLIR SC620) served to observe the change of temperature fields and the emissivity was calibrated and set as 0.98. The room temperature was at 11 Celsius degrees. Numerical simulation with finite-element method was also conducted for further verification of our thermal bilocation design. All the structural parameters as well as the anisotropic thermal conductivity in the corresponding region were in line of the experiments. In addition, the power density of heat sources was equal to that of the square ceramic heaters in experiments. The left and right boundaries were maintained at about 3 °C (due to the influence of room temperature) and the other two boundaries were kept insulated. The surface of device is in thermal convection condition with heat convection coefficient of 5 W/(m^2 K) and ambient temperature of 11 °C. Unstructured tetrahedral grids were built with a minimum grid size of 0.06–0.13.

4. Result and discussion

4.1. Implementation of thermal bilocation camouflage

The simulative results of the asymmetry design are shown as Fig. 4(a)–(c). The simulative and experimental results of the symmetry one are displayed in Fig. 4(d)–(f), and Fig. 4(h)–(j), respectively. The final fabricated prototypes are also shown in Fig. 4 (k)–(m), where the red rectangles in solid line and yellow rectangles in dash line respectively denote the original target heat source and ideal twinborn heat sources, and the blue rectangle in solid line denotes the thermal bilocation region. Without thermal bilocation devices (the first row), the heat sources are located at the center region with more concentrated temperature profiles in both simulations and experiments. When the thermal bilocation devices begin to work (the second row), the temperature profiles are broadened in the center region and the temperature gradients at

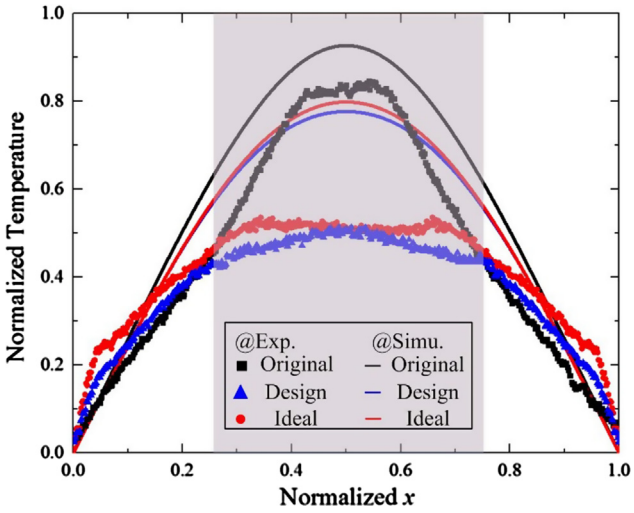

Fig. 5. Temperature curves along the x-axis at $y = -50$ mm.

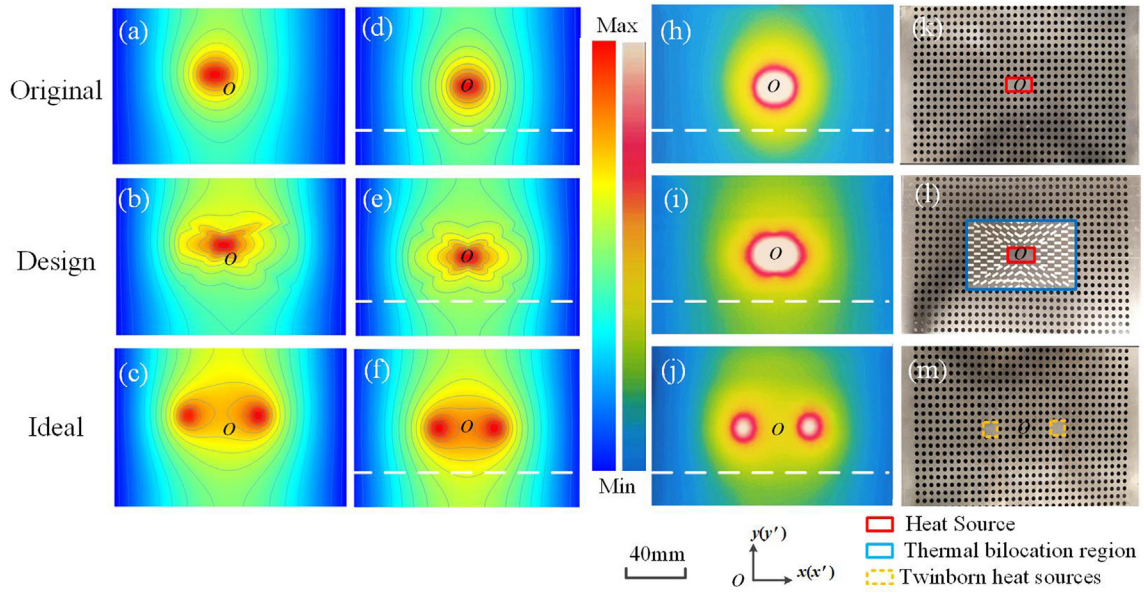

Fig. 4. Temperature profiles of simulations (a)–(c) of the asymmetry design, temperature profiles of simulations (d)–(f) and experiments (h)–(j) of the symmetry design, experimental prototypes (k)–(m) of the symmetry design. The first row denotes the original temperature profiles without the thermal meta-devices; the second row denotes the designed temperature profiles with the thermal meta-devices; the third row denotes the expected ideal temperature profiles.

the two sides near the left and right boundaries arise. The third row shows the expected temperature profiles with separated heat sources. Comparing the asymmetric and the symmetric temperature profiles in the third row with those in the second row, we can find that the temperature profiles approximate with each other outside the bilocation device correspondingly but disagree with the first row, which implies that the devices split heat sources into twinborn heat signatures effectively. This is the exact goal of the present design, which makes it more difficult to judge the actual location from two deceptive heat signatures than just one replaced signature [26]. Furthermore, the bilocation effect can be furthermore improved with more sophisticated design. For instance, we can split and move the heat source into a line configuration or a desired shaped zone while the actual heat source just locates in the line or the zone, which can eliminate the location and effect of the actual heat source indeed. In this sense, the target can be really thermally camouflaged from the IR camera or radar.

To analyze the thermal bilocation effect more quantitatively, we compared the simulative and experimental temperature curves on the same-level white dash lines along the x-axis in Fig. 4(d)–(j) with normalized coordinate and normalized temperature, as shown in Fig. 5. It is clear from Fig. 5 that when the thermal bilocation device is absent, the temperature gradient is almost uniform and the center region has the highest temperature, while when the thermal bilocation device begins to work, the temperature gradient decreases in the center region and arises sharply in the two sides, corresponding to the temperature fields in Fig. 4. Moreover, the temperature curves are similar to each other for the ideal temperature (red curve) and the temperature of the thermal bilocation device (blue curve) in either simulations or experiments, which indicate satisfying thermal camouflage effect outside the device region (the dash lines are outside the device actually). But there is certain deviation between the results of simulations and experiments, which is mainly caused by the inherent deviation of the effective medium theory utilized in experiments, whose accuracy is restricted by the size of the structural unit, as well as the ignorance of the interface resistance in experiments and the inaccuracy of heat convection condition in simulation. From Figs. 4 and 5, the

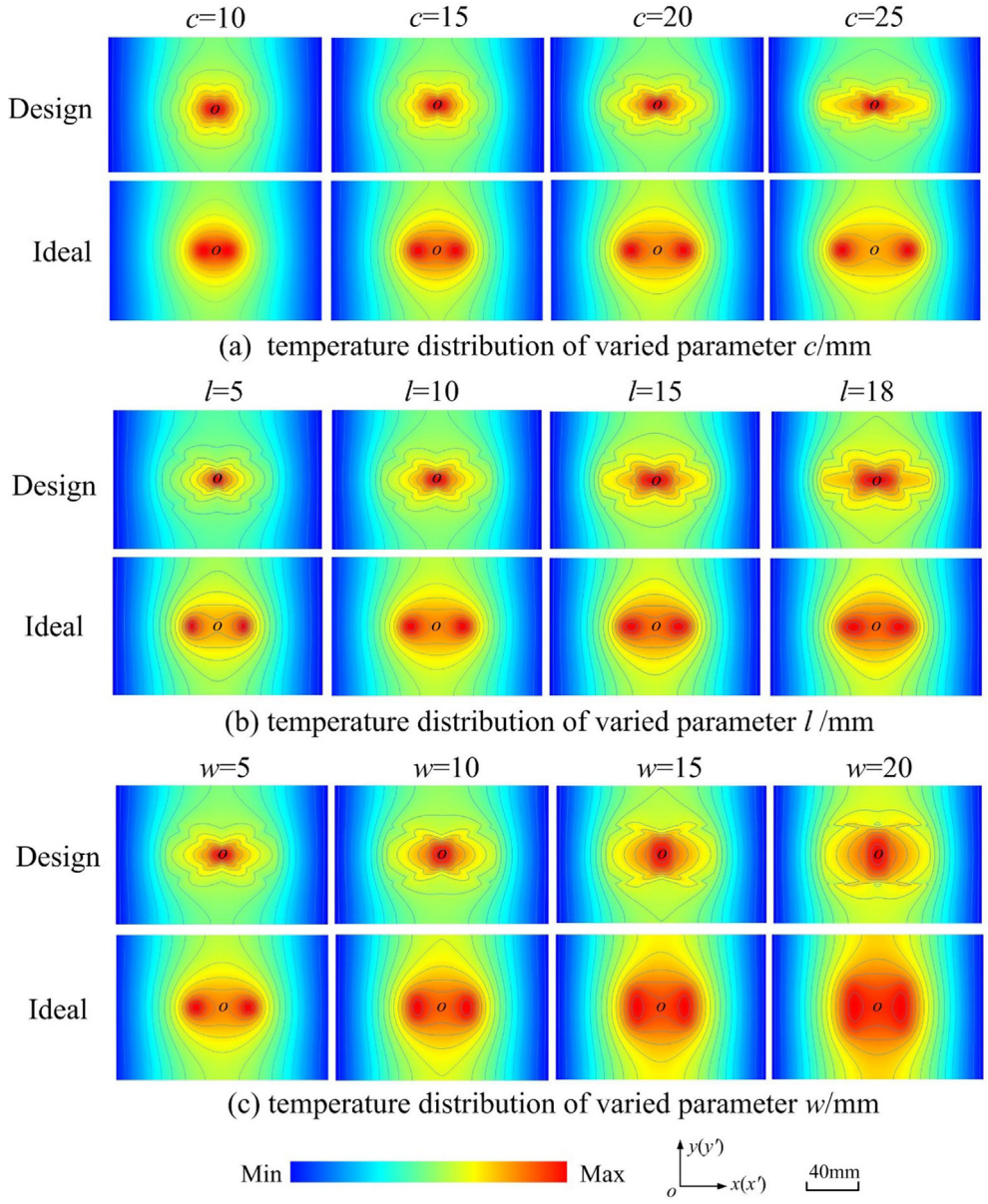

Fig. 6. Temperature profiles of various structure parameters, (a) the separating distances of heat sources c with values of 10, 15, 20, and 25 mm, (b) the lengths of heat sources l with values of 5, 10, 15 and 18 mm, (b) the widths of heat sources w with values of 5, 10, 15 and 20 mm.

results vigorously validate that the thermal bilocation device splits the heat source effectively as designed.

4.2. Performance optimization

To further optimize the thermal bilocation effect, a series of simulations was performed. In our actual thermal bilocation design, $a = b = d = 0$ which means anisotropic thermal conductivities are only determined by the values of L-l, W-w and c. Here we compare the thermal bilocation performance of diverse meta-devices of the same boundary dimensions, length L and width W of the device, and various internal dimensions, like the separating distance c, the length l and the width w of heat sources. To be specific, $L = 40$ mm, $W = 22.3$ mm. We carried out seven simulations of various c and same $l = 10$ mm, $w = 5$ mm, seven simulations of varied l and same $w = 5$ mm, $c = 20$ mm and seven simulations of varied w and the same $l = 10$ mm and $c = 20$ mm. A portion of the simulation results of thermal bilocation devices with different structure parameters, including the separating distance c, the length l and the width w of the heat sources, are plotted as Fig. 6.

Fig. 6(a) shows the temperature distribution of varying separation distance c, whose increase causes the temperature profiles inside the device region to compress along the vertical direction as well as expand farther along the horizontal direction. In Fig. 6 (b), with the length l of the heat source in each row increasing from left to right, the temperature profiles expand more along the horizontal direction inside the device region. Meanwhile, compared with the expected ideal temperature, the temperature agreement of thermal bilocation device seems to increase and the bilocation effect seems be reinforced with increasing l. Depending on the temperature distribution of varying width w, shown as Fig. 6(c), we find that with the enlarging of w, the temperature profiles not only expand farther along the vertical direction inside the device region, but also progressively develop into diverse temperature distribution with unique isotherm.

To more persuasively analyze the influence of varying structure parameters c, l and w, we plotted the distribution diagram of the temperature difference between the design and ideal case in the device, i.e. $\Delta T(x,y) = T_{device}(x,y) - T_{ideal}(x,y)$ as shown in Fig. 7 which has a symmetric color bar meaning the blue region always stands a near-zero temperature. In Fig. 7, the regions' maximum and minimum ΔT are marked out and located at the places of heat sources of design and ideal cases, respectively. Outside the device region, the temperature difference is almost uniform, which indicates the perfect exterior thermal camouflage effect. Based on the presented region of effective thermal bilocation function, we define an area ratio as $\eta = \iint_{|\Delta T|<\varepsilon} dxdy / \iint dxdy$ for quantitative discussion about the influence of the geometric parameters on the thermal bilocation performance, where ε is a small value to denote the critical temperature difference. It is perceived that ε is dependent on the power of heat source and larger ε corresponds to larger area ratio η but makes no difference to the following discussions. In this study, we choose the ε as 0.5. Fig. 8 shows the variation of η by changing thermal bilocation devices with different structure parameters c, l and w. As shown in Fig. 8, with the increasing c and w, the ratio η decreases obviously, corresponding to a shrinking area of effective thermal bilocation function. The red line, as shown in Fig. 8, indicates that, with the increase of the length l of heat source, more heat is diffused along the horizontal direction

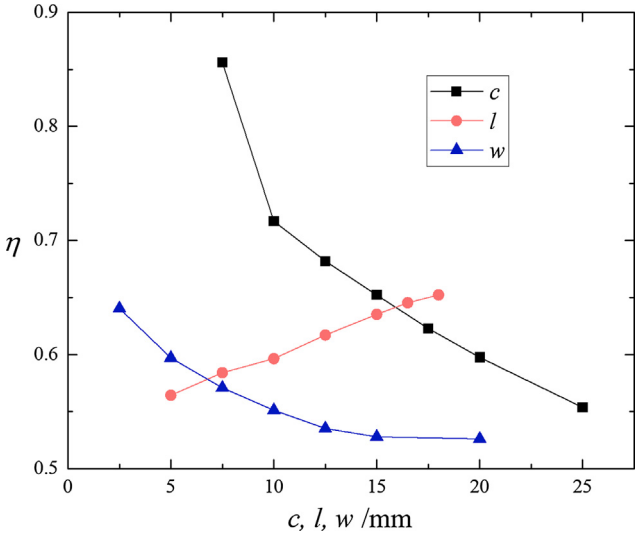

Fig. 8. Dependence of area ratio η on various structure parameters.

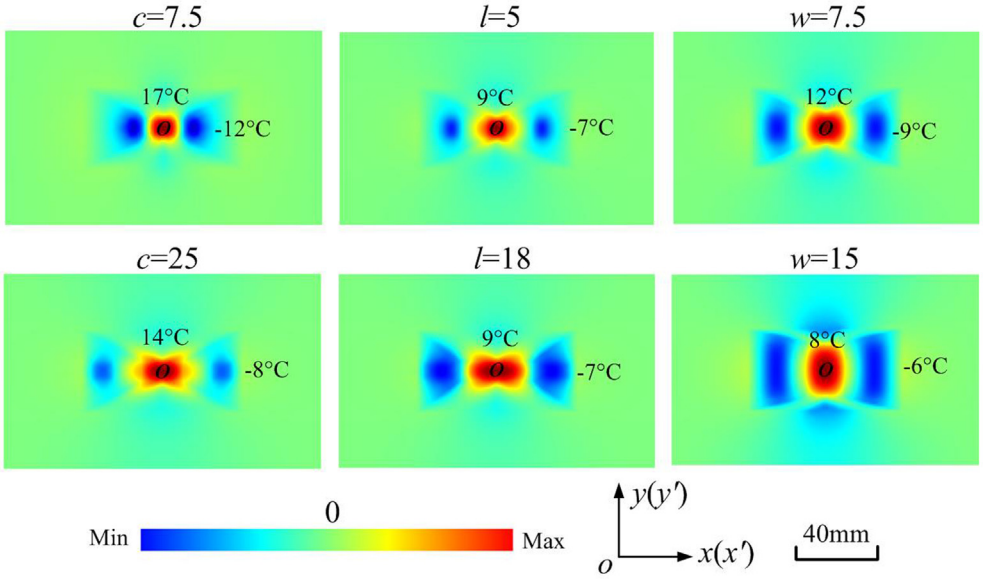

Fig. 7. The distribution diagrams of the temperature differences between the design and ideal cases with various structure parameters.

and the ratio η increases obviously. Both the increase of c and l give rise to the horizontal expansion of thermal illusions of the heat source. On the contrary, the increasing width w of the heat source corresponds to stronger thermal diffusion along the vertical direction. In short, it derives from Fig. 8 that, on the condition of meeting the feasibility, the smaller the structure parameters w and c are or the larger the structure parameter l is, the better the thermal bilocation function is.

5. Conclusions

In summary, we fabricated a device to realize bilocation-like heat signatures for thermal camouflage application and researched the influence of varied structure parameters on thermal bilocation performance. Detailed design and experimental processes were introduced. The experimental and simulated results are in good agreement with each other. And the temperature contours and distribution curves around the device region are of pleasant similarity with those of twinborn heat sources, which successfully verifies the thermal bilocation idea. Furthermore, by carrying out a series of finite-element simulations with varied structure parameters focusing on the thermal bilocation performance, we conclude that the smaller structure parameters c, w, and larger l, the better thermal bilocation function can we achieve. Our thermal bilocation devices can camouflage the target with twinborn-like signatures at different locations, increasing the deceptiveness greatly compared with only thermal relocation or deformation. The present unprecedented function not only can fortify the means of thermal camouflage, but also can arise keen interests to realize the bilocation in other physical fields, such as optics, electromagnetics, acoustics, etc.

Conflict of interest

There are no conflicts of interest.

Acknowledgements

The authors would like to acknowledge the financial support from the National Natural Science Foundation of China (Grant Nos. 51606074 and 51625601), the Ministry of Science and Technology of the People's Republic of China (Project No. 2017YFE0100600), and the National Key Research and Development Program of China (Project Nos. 2016YFB0400804).

Appendix A. Supplementary material

Supplementary data associated with this article can be found, in the online version, at https://doi.org/10.1016/j.ijheatmasstransfer.2018.07.034.

References

[1] U. Leonhardt, Optical conformal mapping, Science 312 (5781) (2006) 1779–1780.
[2] D. Schurig, J. Pendry, D.R. Smith, Transformation-designed optical elements, Opt. Exp. 15 (22) (2007) 14772–14782.
[3] C. Fan, Y. Gao, J. Huang, Shaped graded materials with an apparent negative thermal conductivity, Appl. Phys. Lett. 92 (2008) 251907.
[4] T. Chen, C. Weng, J. Chen, et al., Cloak for curvilinearly anisotropic media in conduction, Appl. Phys. Lett. 93 (2008) 114103.
[5] J. Li, Y. Gao, J. Huang, A bifunctional clock using transformation media, J. Appl. Phys. 108 (2010) 074504.
[6] S. Guenneau, C. Amra, D. Veynante, Transformation thermodynamics: cloaking and concentrating heat flux, Opt. Exp. 20 (7) (2012) 8207–8218.
[7] S. Narayana, Y. Sato, Heat flux manipulation with engineered thermal materials, Phys. Rev. Lett. 108 (2012) 214303.
[8] R. Schittny, M. Kadic, S. Guenneau, et al., Experiments on transformation thermodynamics: molding the flow of heat, Phys. Rev. Lett. 110 (2013) 195901.
[9] Y. Ma, L. Lan, W. Jiang, et al., A transient thermal cloak experimentally realized through a rescaled diffusion equation with anisotropic thermal diffusivity, NPG Asia Mater. 5 (2013) e73.
[10] X. He, L. Wu, Design of two-dimensional open cloaks with finite material parameters for thermodynamics, Appl. Phys. Lett. 102 (2013) 211912.
[11] H. Xu, X. Shi, F. Gao, et al., Ultrathin three-dimensional thermal cloak, Phys. Rev. Lett. 102 (2014) 054301.
[12] T. Han, X. Bai, D. Gao, et al., Experimental demonstration of a bi-layer thermal cloak, Phys. Rev. Lett. 112 (2014) 054302.
[13] Y. Zhang, H. Xu, B. Zhang, Design, implementation, and extension of thermal invisibility cloaks, AIP Adv. 5 (2015) 053402.
[14] G. Xu, H. Zhang, A concept of heat dissipation coefficient for thermal cloak based on entropy generation approach, AIP Adv. 6 (9) (2016) 095107.
[15] R. Hu, B. Xie, J. Hu, et al., Carpet thermal cloak realization based on the refraction law of heat flux, EPL 111 (2015) 54003.
[16] E.M. Dede, T. Nomura, P. Schmalenberg, et al., Heat flux cloaking, focusing, and reversal in ultra-thin composite considering conduction-convection effects, Appl. Phys. Lett. 103 (2013) 063501.
[17] S. Guenneau, C. Amra, Anisotropic conductivity rotates heat fluxes in transient regimes, Opt. Exp. 21 (5) (2013) 6578–6583.
[18] R. Hu, X. Wei, J. Hu, et al., Local heating realization by reverse thermal cloak, Sci. Rep. 4 (2014) 3600.
[19] Y. Li, X. Shen, Z. Wu, et al., Temperature-dependent transformation thermotics: from switchable thermal cloaks to macroscopic thermal diodes, Phys. Rev. Lett. 115 (2015) 195503.
[20] R. Hu, S. Zhou, W. Shu, et al., Directional heat transport through thermal reflection meta-device, AIP Adv. 6 (2016) 125111.
[21] R.S. Kapadia, P.R. Bandaru, Heat flux concentration through polymeric thermal lenses, Appl. Phys. Lett. 105 (2014) 233903.
[22] Y. Liu, F. Sun, S. He, Novel thermal lens for remote heating/cooling designed with transformation optics, Opt. Exp. 24 (6) (2016) 5683–5692.
[23] X. Shen, Y. Li, C. Jiang, et al., Temperature trapping: energy-free maintenance of constant temperatures as ambient temperature gradients change, Phys. Rev. Lett. 117 (2016) 055501.
[24] T. Han, X. Bai, J. Thong, et al., Full control and manipulation of heat signatures: cloaking, camouflage and thermal metamaterials, Adv. Mater. 26 (2014) 1731–1734.
[25] T. Yang, Y. Su, W. Xu, et al., Transient thermal camouflage and heat signature control, Appl. Phys. Lett. 109 (2016) 121905.
[26] Q. Hou, X. Zhao, T. Meng, et al., Illusion thermal device based on material with constant anisotropic thermal conductivity for location camouflage, Appl. Phys. Lett. 109 (2016) 103506.
[27] Y. Li, X. Bai, T. Yang, et al., Structured thermal surface for radiative camouflage, Nat. Commun. 9 (2018) 273.
[28] G. Dai, J. Shang, J. Huang, Theory of transformation thermal convection for creeping flow in porous media: cloaking, concentrating, and camouflage, Phys. Rev. E 97 (2018) 022129.
[29] T. Chen, F. Yang, Z. Mei, A simple and flexible thermal illusion device and its experimental verification, Phys. Stat Solidi A. 212 (2015) 1746–1750.
[30] N. Zhu, X. Shen, J. Huang, Converting the patterns of local heat flux via thermal illusion device, AIP Adv. 5 (2015) 053401.
[31] R. Hu, S. Zhou, Y. Li, et al., Illusion thermotics, Adv. Mater. (2018) 1707237.
[32] https://en.wikipedia.org/wiki/Bilocation.
[33] E.M. Dede, T. Nomura, P. Schmalenberg, et al., Heat flux cloaking, focusing, and reversal in ultra-thin composites considering conduction-convection effects, Appl. Phys. Lett. 103 (6) (2013) 063501.
[34] P.R. Bandaru, K.P. Vemuri, F.M. Canbazoglu, et al., Layered thermal metamaterials for the directing and harvesting of conductive heat, AIP Adv. 5 (2015) 053403.
[35] N. Athanasopoulos, N.J. Siakavellas, Heat manipulation using highly anisotropic pitch-based carbon fiber composites, Adv. Eng. Mater. 17 (10) (2015) 1494–1503.
[36] R. Hu, S. Zhou, X. Yu, et al., Exploring the proper experimental conditions in 2D thermal cloaking demonstration, J. Phys. D: Appl. Phys. 49 (2016) 415302.
[37] C. Yuan, B. Duan, L. Li, et al., Thermal conductivity of polyer-based composites with magnetic aligned hexagonal boron nitride platelets, ACS Appl. Mater. Inter. 7 (2015) 13000–13006.